



CHAPTER 7

FINAL CONCLUSIONS

7.1 CONCLUSIONS	273
7.2 PERSPECTIVES	278

7.1 CONCLUSIONS

The characterisation of the most novel metallofullerenes up to 2004 has been theoretically and systematically discussed in various chapters of this study. Fullerenes that do not contain metals can be successfully characterized with semiempirical methods, but metallofullerenes require DFT-based methods. These methods provide an interesting framework for performing first-principle calculations of large systems more cheaply than post-HF methods. In the near future, the rapid increase in computer development and the implementation of new algorithms as well as new functionals will provide more powerful tools to scientists for studying the electronic structure of the new metallofullerenes. The way forward has already been initiated.

The vigorous start to fullerene chemistry may seem to have stopped at the end of the 1990s since several authors had already established its chemical principles. Manolopoulos et al. systematized the isomerism in the free fullerenes, and Taylor and Hirsch determined the procedure for

predicting chemical reactivity. Only the appearance of new compounds with unexpected properties and reactivity has given rise to a certain resurgence of fullerene chemistry. Two of these novel compounds are fullerenes that encapsulate a metal unit of four atoms and fullerenes that some carbons are substituted by metals. Both are metallofullerenes. From the structural point of view, metallofullerenes can be divided into three main groups, all of which have been discussed in this study: endohedral, heterohedral and exohedral metallofullerenes. The main families of compounds studied are $\text{Sc}_{3-n}\text{M}_n\text{N}@C_k$ ($n = 0-3$, $\text{M} = \text{Y, La}$; $k = 68, 78, 80$) (endohedral), C_xM_n ($x = 56, 57, 58, 59$; $\text{M} = \text{Pt, Ir, Os}$; $n = 1, 2$) (heterohedral) and $(\eta^2\text{-C}_k)\{\text{M}(\text{PH}_3)_2\}_n$ ($k = 60, 70, 84$; $\text{M} = \text{Pt, Pd, Ni}$; $n = 1, 2, 4, 6$) (exohedral). The present study is a step forward in our knowledge of each of these families of compounds, and in particular, in our understanding of the metal-carbon bond, isomerism and reactivity. The DFT method proved to be an excellent computational tool for providing good geometries, for solving the intricacies of the different metal-carbon bonds, for producing experimental data (ionization potentials and electron affinities) and also for making predictions about isomerism stability and reactivity. The principal conclusions drawn about the species studied here are:

The experimental advances in each field have not been homogeneous. In consequence, the information available for each family of compounds is completely different. Whereas exohedral metallofullerenes were the first metallofullerenes to be studied in depth and their macroscopic quantities had allowed their characterisation by X-ray crystallography and other spectroscopic techniques, heterohedral metallofullerenes are still in their infancy because they have only been detected in tiny quantities by mass spectrometric studies. In the case of TNT endohedral metallofullerenes, huge advances have been made in recent years and they can now be synthesised in bulk quantities. Some of TNT endohedral metallofullerenes have been fully characterised by X-ray, IR and UV-vis techniques.

Many years studying metallofullerenes from a theoretical point of view. At first, fullerene chemistry was written about from the perspective of organic and physical chemistry and also materials science. It was not until

the middle 1990s that inorganic/organometallic chemistry began to take part. The most important characteristic of fullerenes is their ability to react as poorly conjugated and electron-deficient alkenes. Hence, fullerenes can be readily reacted with electron-rich metal species such as nucleophiles, bases, radicals or reducing agents. The perfect combination of fullerenes and metallic units has produced an endless variety of different stoichiometries for metallofullerenes. The first to be detected was the La@C₆₀ endohedral metallofullerene and the first to be studied was the exohedral metallofullerene C₆₀(t-BuC₅H₅N)₂OsO₄.

Different types of structures, different types of metal-carbon bonds.

The metal units in each family of compounds are located differently in relation to the fullerene carbon framework: inside the cage, within the carbon framework and outside the cage. Each metal position is characterized by a different number of carbon neighbours and is also at different M–C bond lengths. These differences mean that the metal–carbon bond in each family of metallofullerenes has different models. The encapsulation of a trimetallic nitride template unit (TNT, Sc_{3-*n*}M_{*n*}N; *n* = 0-3; M = Y, La) inside the carbon cage to produce TNT endohedral metallofullerenes is explained by an ionic pair (cage-metal) model in which the TNT unit formally transfers six electrons to the cage. Classical endohedral metallofullerenes can also be explained mostly by an ionic model but when other bonding models appear when the guest is bigger or the host have not a big enough hollow (*e.g.* C₂₈). On the other hand, in heterohedral metallofullerenes, metals establish a covalent metal-carbon bond without causing oxidation to the metal. Finally, the (MPH₃)₂ metal units situated exohedrally to the fullerene are only coordinated in a η^2 mode to the C–C bond. However, stronger metal-carbon bonds are found in other exohedral metallofullerenes when a different metal unit is involved. For example: {Re(CO)₅}₂ and O₂OsO₂(4-Bu^tC₅H₄N)₂. This means that exohedral metallofullerenes can be classified as π - and σ -bonded metal-fullerene complexes. The former (studied here) are π -bonded exohedral metallofullerenes whereas the latter are σ -bonded exohedral metallofullerenes. The different strength of each metal-carbon bond can be exemplified by the magnitude and sign of the binding energies of the formation reaction of the endohedral, heterohedral and exohedral metallofullerenes: –11.60 eV for the encapsulation reaction

$\text{Sc}_3\text{N} + \text{C}_{80} \rightarrow \text{Sc}_3\text{N@C}_{80}$; 7.35 eV for the substitution reaction $\text{Pt} + \text{C}_{60} \rightarrow \text{C}_{58}\text{Pt} + \text{C}_2$; and -0.96 eV for the coordination reaction $\text{Pt}(\text{PH}_3)_2 + \text{C}_{60} \rightarrow (\eta^2\text{-C}_{60})\text{Pt}(\text{PH}_3)_2$.

Chemometric tools applied to isomerism studies. Classical methodology (which pre-determines all the isomers that are to be calculated) is used to study the isomerism in endohedral and exohedral metallofullerenes. It has been successful because the number of isomers is very limited. Nevertheless, the regioisomers of heterohedral metallofullerenes can be much more numerous: for example, the stoichiometry C_{57}Pt_2 has 43 distinct regioisomers. Thus, other techniques which can manage considerable amounts of data must be used if we want to understand regioisomerism in heterohedral metallofullerenes. Also, we are interested in the factors that govern the stability of isomers. As regard to this, chemometric tools have been very useful for drawing conclusions from the considerable quantities of data provided by the factors which affect the stability of regioisomers. These tools have been used not only for analysing data but also for predicting the stability of other heterofullerenes.

TNT encapsulation stabilizes fullerene isomers that are not available as free fullerenes. TNT endohedral metallofullerenes are formed by the encapsulation of a metallic nitride template inside the following cages: $D_3\text{-C}_{68}$:**6140**, $D_{3h}\text{-C}_{78}$:**5**, $D_{5h}\text{-C}_{80}$:**6** and $I_h\text{-C}_{80}$:**7**. The $D_{3h}\text{-C}_{78}$:**5** and $I_h\text{-C}_{80}$:**7** cages have never been detected experimentally because these cages are not the most stable IPR isomers for C_{78} and C_{80} stoichiometries. Even the C_{68} fullerene is not an IPR fullerene, which means that atom for atom it is less stable than the IPR fullerenes. So, endohedral metallofullerenes can make non-classical fullerene isomers available for study. Furthermore, on the basis of the electronic structure we predicted that no other IPR fullerenes between C_{60} and C_{84} will be capable of encapsulating a TNT unit, apart from the fullerene isomers that are already known. TNT encapsulations keep open for the non-IPR fullerenes. This is because only free fullerene isomers with a high LUMO+3-LUMO+4 gap can encapsulate and stabilize metal units that formally transfer six electrons to the cage. The only free fullerene isomers that obey this rule are the abovementioned cages.

Stability of the carbon skeleton is the principal factor that determines the regioisomer stability of the heterofullerenes. DFT calculations carried out on numerous regioisomers of $C_{57}Pt_2$ and $C_{56}Pt_2$ clearly show that the metal atoms occupy neighbouring positions in the most stable structures. Metal substitution deforms the carbon framework and partially destroys the fullerene aromaticity. This is the *key* factor in determining the stability of these disubstituted clusters. Indeed, it is much easier to make a big hole that permits the incorporation of two Pt atoms in the carbon cage than two smaller holes in two opposite sites of the fullerene. The structures with two neighbouring Pt atoms retain the most C–C bonds, which is another important factor in determining the stability of the cluster. In addition, clusters with short Pt–Pt contacts may contain weak metal-metal interactions, which also favor the stability of the cluster but are not a fundamental stability element. In our opinion, these results go beyond the particular cases of the $C_{57}Pt_2$ and $C_{56}Pt_2$ regioisomers and we believe that the present conclusions can be extended to any transition metal derivative. Calculations performed on the ionic species of the Pt-derivatives and on some Ti homologues confirm the hypothesis that disubstituted C_{60} fullerenes contain the heteroatoms in adjacent sites. The behaviour of larger fullerenes such as C_{70} , should be similar although in this case the curvature of the fullerene could also be important.

Prediction of the exohedral reactivity taking into account the full characterization of the different C–C bond types. In order to predict the exohedral reactivity of a fullerene cage such as endohedral metallofullerenes and free fullerenes, we first performed a full characterization of all C–C bond types. The fullerenes characterized were: I_h-C_{60} :**1**, D_3-C_{68} :**6140**, $D_{5h}-C_{70}$:**1**, $D_{3h}-C_{78}$:**5**, I_h-C_{80} :**7**, D_2-C_{84} :**22** and $D_{2d}-C_{84}$:**23**. Each C–C bond type is characterized by its topology, length, pyramidalization angle and Mayer bond order. This systematization enabled us to identify which sites were most reactive to a nucleophilic addition to free fullerenes or a [4 + 2] cycloaddition to TNT endohedral metallofullerenes. They are the most pyramidalized C–C bonds that also have a high Mayer bond order. However, these features are often not found simultaneously and so the most reactive site is usually a compromise between a highly pyramidalized C–C bond with a lower pyramidalization angle, and a C–C bond with a high

Mayer bond order but a lower pyramidalization angle. The most reactive site always goes to the pyracylene 6:6 C–C bond types.

Metal doping as a tool for modifying physical properties. In general, fullerenes have relatively large electron affinities and ionization potentials, because of the presence of low-lying unoccupied and occupied orbitals, respectively. The endohedral and heterohedral functionalization can modify these physical properties because these transformations change the electronic structure of fullerenes. It is interesting to see that heterohedral and endohedral metal doping reduce the ionization potentials, making the fullerenes better electron-donor compounds. Endohedral TNT doping reduces the EA of the fullerene whereas heterohedral metal doping increases and thus improves the electron acceptor character of free fullerenes.

7.2 PERSPECTIVES

Without doubt, the main theoretical challenges in the field of metallofullerenes are provided by heterohedrals and endohedrals. To date, only simple stoichiometries have been studied: those with a single carbon atom or C₂ unit replaced by a metal atom. But other structures, which are created by the loss of C₂ units in the former, have still to be studied. There are two main experimental methods for producing heterohedral metallofullerenes: (1) Branz's method, which involves gas phase clusters: C₆₀M_n and (2) Balch's method, which involves polymeric, covalently bound chains: ...C₆₀ML_n·C₆₀ML_n.... Depending on the production method different stoichiometries may be preferred. So Branz's method tends to produce carbon cages with an odd number of carbons whereas Balch's method produces higher yields of carbon cages with an even number of carbons. So the mechanism for forming heterohedral metallofullerenes remains unsolved. On the other hand, theoreticians are waiting for experimental evidence of metal doping in other fullerenes such as C₇₀, C₇₈, C₈₀ or C₈₄ which exist as free fullerenes. These fullerenes will make it possible to study the effect of substituting C–C bonds with different pyramidalization angles in the problem of the regioisomerism. Furthermore, the fact that the variability in the topology and bond strength of higher fullerenes is greater than that of the two previously studied C–C bonds of

the C_{60} will give us the final clues about the factors which govern the regioisomerism.

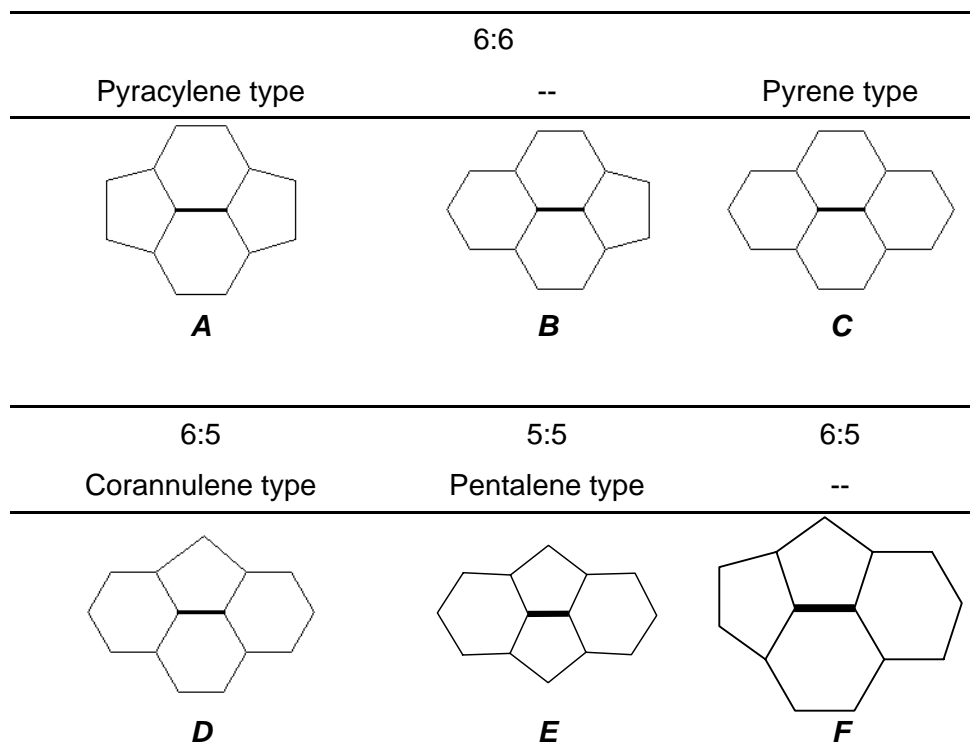
Apparently no more TNT endohedral metallofullerenes will be synthesized from IPR isomers between C_{60} and C_{84} . Researchers should focus on discovering new non-IPR cages which can encapsulate these TNT units. This is interesting because TNT encapsulation can make fullerene cages available that would otherwise remain unstable. To date only endohedral metallofullerenes can do this. Theoreticians should also pay greater attention to exohedral reactivity. Some progress in this area has already been made for $Sc_3N@C_{80}$. But, the exohedral reactivity of $Sc_3N@C_{68}$ and $Sc_3N@C_{78}$ complexes is almost completely unknown. Although progress in this research area is very fast, there are still many open questions concerning the electronic structure of the classical endohedral metallofullerenes such as $M_2@C_{80}$ ($M = La, Ti$). In the case of exohedral metallofullerenes, it seems necessary to focus on how the computational effort can be reduced before moving on to new and bigger fullerene complexes with metal units added exohedrally.

appendix

A.1 GENERAL DESCRIPTION	282
A.2 I_h-C_{60}:1.....	283
A.3 D_3-C_{68}:6140	284
A.4 $D_{5h}-C_{70}$:1	286
A.5 $D_{3h}-C_{78}$:5	287
A.6 I_h-C_{80}:7	289
A.7 D_2-C_{84}:22	290
A.8 $D_{2d}-C_{84}$:23	292
REFERENCES AND NOTES	293

A.1 GENERAL DESCRIPTION

All different C–C bonds types in IPR fullerenes (*A–D* types) and two additional types found in the non-IPR D_3-C_{68} (*E* and *F* types). The bold line determines the considered C–C bond. The 6:6 ring junction in the *A* type is abutted by two pentagons (pyracylene C–C bond type), by a hexagon and a pentagon in the *B* type and by two hexagons in the *C* type (pyrene C–C bond type). The *D* type is called corannulene C–C bond type and represents a 6:5 ring junction abutted by two hexagons. The *E* type called pentalene C–C bond type is a 5:5 ring junction abutted by two hexagons and the *F* type is a 6:5 ring junction abutted by a pentagon and a hexagon. The two last types (the *E* and *F* types) are very destabilizing and only found in non-IPR fullerenes.

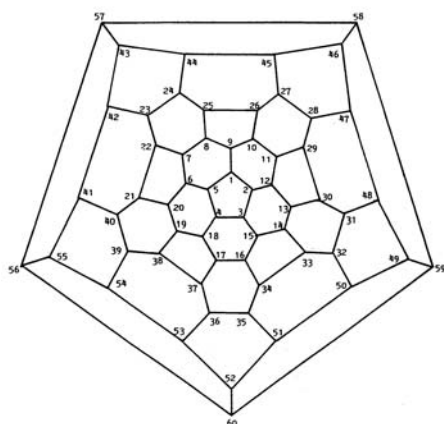


A.2 I_h -C₆₀:1

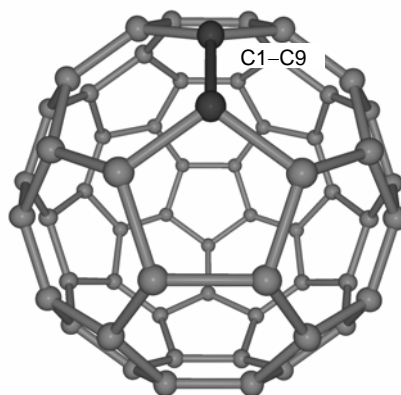
Description of the 90 C–C bonds of the I_h -C₆₀:1 IPR fullerene divided into 2 non-equivalent sets

<i>C–C bond</i> ¹	<i>Ring junction</i>	<i>Type</i> ²	<i>Bond lengths</i> (Å)	θ_p (°) ³	<i>MBO</i> ⁴
1,9/66	6:6	pyracylene, A	1.397	11.67	1.342
1,2/65	6:5	corannulene, D	1.452	11.67	1.136

Schlegel diagram showing the numbering system for I_h -C₆₀:1 (a) and the structure with the C1–C9 bond marked (b)



(a) Schlegel diagram of I_h -C₆₀:1



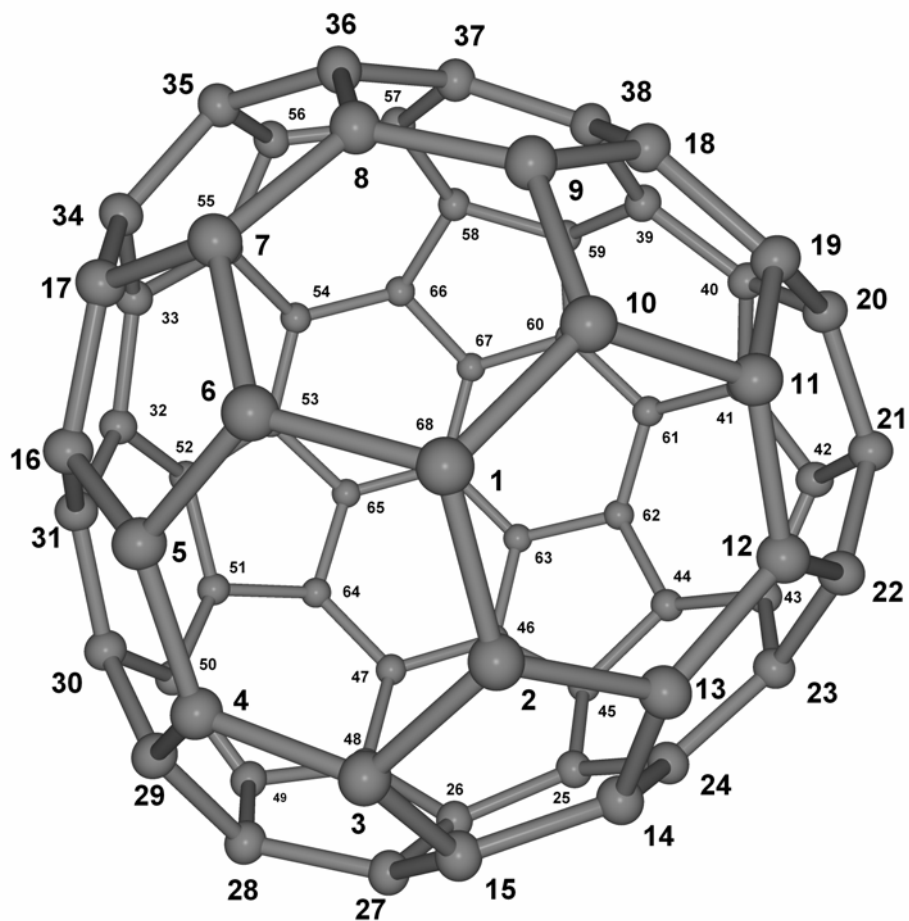
(b) Structure of I_h -C₆₀:1

A.3 D_3 -C₆₈:6140

Description of 102 C–C bonds of the D_3 -C₆₈:6140 non-IPR isomer divided into 18 non-equivalent sets

<i>C–C bond</i>	<i>Ring junction</i>	<i>Type</i> ²	<i>Bond lengths</i> (Å)	θ_p (°) ³	<i>MBO</i> ⁴
15,27	6:6	pyracylene, A	1.396	11.52	1.266
23,24	6:6	B	1.418	9.93	1.257
14,24	6:6	B	1.429	9.71	1.252
12,13	6:6	B	1.413	9.72	1.247
11,12	6:6	B	1.433	10.48	1.235
21,22	6:5	F	1.421	13.77	1.224
1,2	6:6	B	1.431	9.58	1.215
2,3	6:5	corannulene, D	1.433	10.90	1.210
22,23	6:5	corannulene, D	1.450	11.31	1.199
13,14	6:5	corannulene, D	1.443	10.54	1.194
20,21	6:5	F	1.424	14.49	1.185
3,15	6:5	corannulene, D	1.447	11.27	1.165
2,13	6:5	corannulene, D	1.449	10.14	1.159
21,42	5:5	E	1.436	16.20	1.156
12,22	6:6	B	1.446	10.27	1.151
26,27	6:5	corannulene, D	1.458	11.78	1.136
14,15	6:5	corannulene, D	1.438	10.80	1.133
24,25	6:6	pyrene, C	1.488	8.58	1.118

Structure of the D_3 - C_{68} :**6140** non-IPR isomer showing the numbering system

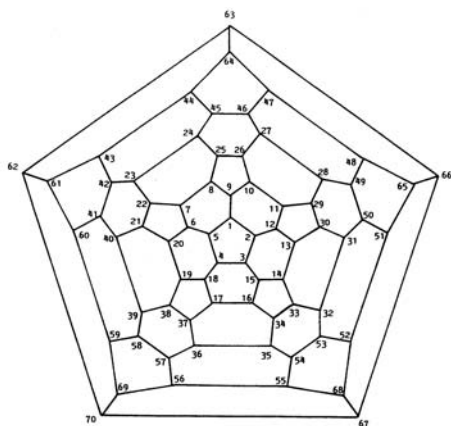
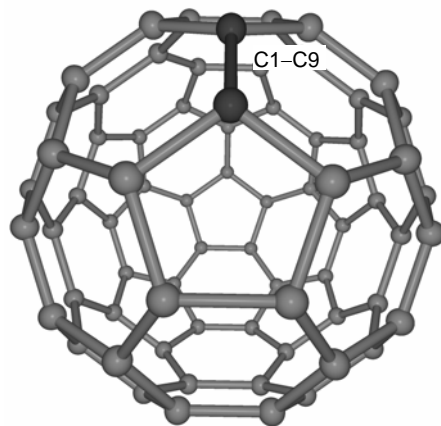


A.4 D_{5h} -C₇₀:1

Description of 105 C–C bonds of the D_{5h} -C₇₀:1 IPR isomer divided into 8 non-equivalent sets

<i>C–C bond</i> ¹	<i>Ring junction</i>	<i>Type</i> ²	<i>Bond lengths</i> (Å)	θ_p (°) ³	<i>MBO</i> ⁴
1,9/ <i>a,b</i>	6:6	pyracylene, A	1.399	11.92	1.334
7,8/ <i>c,c</i>	6:6	pyracylene, A	1.393	11.49	1.332
21,40/ <i>d,e</i>	6:6	B	1.421	9.43	1.246
21,22/ <i>d,d</i>	6:5	corannulene, D	1.438	10.28	1.219
23,24/ <i>e,e</i>	6:6	pyrene, C	1.470	8.60	1.167
6,7/ <i>b,c</i>	6:5	corannulene, D	1.448	11.73	1.140
1,2/ <i>a,a</i>	6:5	corannulene, D	1.451	11.85	1.138
7,22/ <i>c,d</i>	6:5	corannulene, D	1.446	10.88	1.138

Schlegel diagram showing the numbering system for D_{5h} -C₇₀:1 (a) and structure with the C1–C9/Ca–Cb bond marked (b)

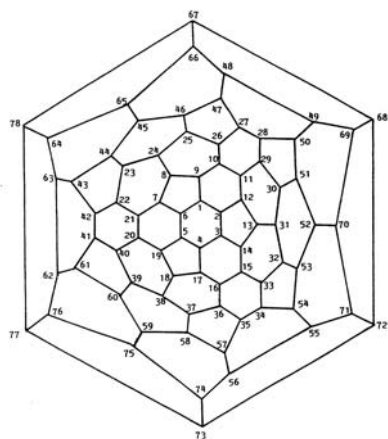
(a) Schlegel diagram of D_{5h} -C₇₀:1(b) Structure of D_{5h} -C₇₀:1

A.5 D_{3h} - C_{78} :5

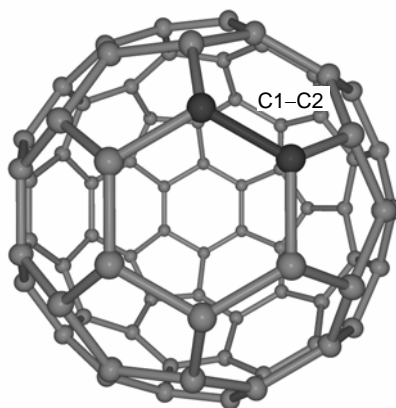
Description of the 117 C–C bonds of the D_{3h} - C_{78} :5 IPR isomer divided into
13 non-equivalent sets

<i>C–C bond</i> ¹	<i>Ring junction</i>	<i>Type</i> ²	<i>Bond lengths</i> (Å)	θ_p (°) ³	<i>MBO</i> ⁴
1,2	6:6	pyracylene, A	1.392	11.67	1.392
27,28	6:6	pyracylene, A	1.372	10.47	1.373
22,23	6:5	corannulene, D	1.414	10.49	1.293
7,21	6:6	B	1.419	9.63	1.283
23,24	6:6	B	1.423	9.56	1.221
8,24	6:6	B	1.424	9.48	1.214
10,26	6:6	B	1.436	9.65	1.205
7,8	6:5	corannulene, D	1.443	10.39	1.195
10,11	6:6	pyrene, C	1.470	8.63	1.163
1,6	6:5	corannulene, D	1.443	11.67	1.158
1,9	6:5	corannulene, D	1.446	11.15	1.129
22,42	6:5	corannulene, D	1.451	10.57	1.111
23,44	6:5	corannulene, D	1.470	10.31	1.090

Schlegel diagram showing the numbering system for D_{3h} - $C_{78}:5$ (a) and structure with the C1–C2 bond marked (b)



(a) Schlegel diagram of D_{3h} - $C_{78}:5$



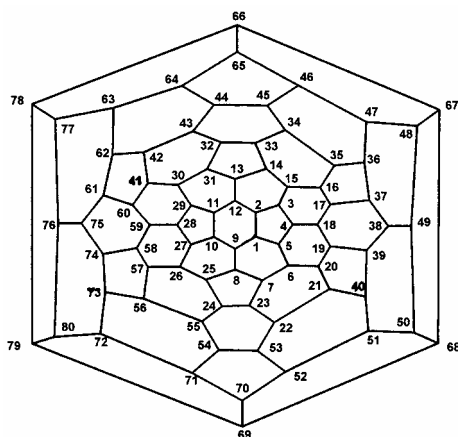
(b) Structure of D_{3h} - $C_{78}:5$

A.6 I_h -C₈₀:7

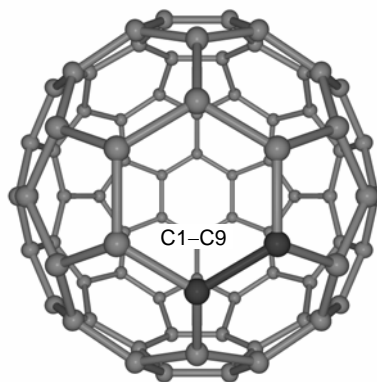
Description of the 120 C–C bonds of the I_h -C₈₀:7 IPR isomer divided into 2 non-equivalent sets⁵

C–C Bond ¹	Ring junction	Type ²	Bond lengths (Å)	θ_p (°) ³	MBO ⁴
1,9/66	6:6	B	1.428	9.62	1.209
1,2/65	6:5	corannulene, D	1.438	10.58	1.194

Schlegel diagram showing the numbering system for I_h -C₈₀:7 (a) and structure with the C1–C9 bond marked (b)



(a) Schlegel diagram of I_h -C₈₀:7



(b) Structure of I_h -C₈₀:7

A.7 D_2 -C₈₄:22

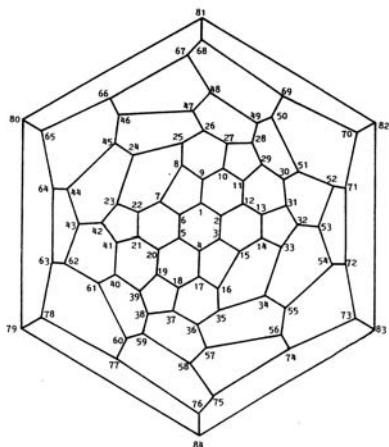
Description of the 126 C–C bonds of the D_2 -C₈₄:22 IPR isomer divided into 32 non-equivalent sets

<i>C–C bond</i> ¹	<i>Ring junction</i>	<i>Type</i> ²	<i>Bond lengths, Å</i>	θ_p (°) ³	<i>MBO</i> ⁴
9,10	6:6	pyracylene, A	1.373	10.73	1.362
32,53	6:6	pyracylene, A	1.369	10.71	1.347
7,22	6:6	pyracylene, A	1.377	10.91	1.326
23,24	6:6	B	1.418	9.31	1.321
8,25	6:6	B	1.418	9.27	1.318
12,13	6:6	B	1.416	9.67	1.266
11,29	6:5	corannulene, D	1.425	10.38	1.249
2,3	6:6	B	1.421	9.59	1.261
26,47	6:6	B	1.409	8.82	1.255
27,28	6:5	corannulene, D	1.427	10.28	1.243
30,31	6:6	B	1.427	9.34	1.252
3,4	6:5	corannulene, D	1.426	10.54	1.239
39,40	6:6	B	1.414	8.88	1.253
26,27	6:6	B	1.426	9.38	1.248
1,2	6:6	B	1.423	9.59	1.248
11,12	6:6	B	1.423	9.69	1.244
13,31	6:5	corannulene, D	1.430	10.73	1.226
7,8	6:5	corannulene, D	1.431	10.86	1.178
24,25	6:6	pyrene, C	1.463	7.67	1.190
14,33	6:5	corannulene, D	1.431	10.94	1.169
2,12	6:6	pyrene, C	1.469	8.64	1.154
24,45	6:6	pyrene, C	1.466	7.76	1.152
25,26	6:6	pyrene, C	1.465	7.81	1.155
31,32	6:5	corannulene, D	1.443	10.74	1.138

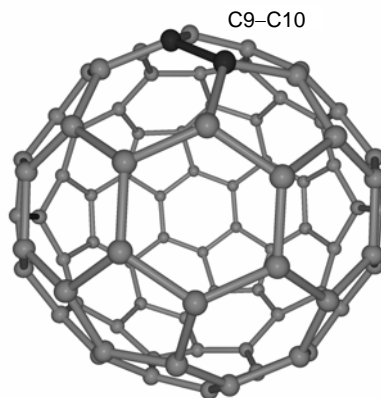
Continue

23,42	6:5	corannulene, <i>D</i>	1.445	10.84	1.128
10,27	6:5	corannulene, <i>D</i>	1.439	10.80	1.130
10,11	6:5	corannulene, <i>D</i>	1.444	10.78	1.125
8,9	6:5	corannulene, <i>D</i>	1.449	10.76	1.121
1,9	6:5	corannulene, <i>D</i>	1.450	10.63	1.124
13,14	6:5	corannulene, <i>D</i>	1.452	10.80	1.122
28,29	6:5	corannulene, <i>D</i>	1.454	9.79	1.110
3,15	6:5	corannulene, <i>D</i>	1.453	10.73	1.111

Schlegel diagram showing the numbering system for D_2 -C₈₄:**22** (a) and structure with the C9–C10 bond marked (b)



(a) Schlegel diagram of D_2 -C₈₄:**22**



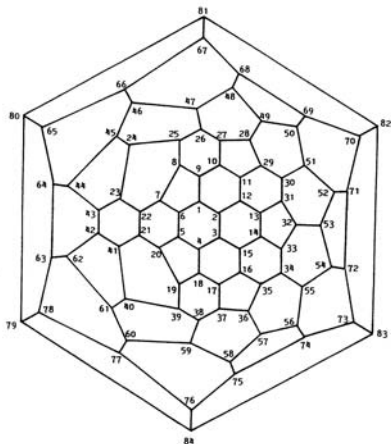
(b) Structure of D_2 -C₈₄:**22**

A.8 D_{2d} -C₈₄:23

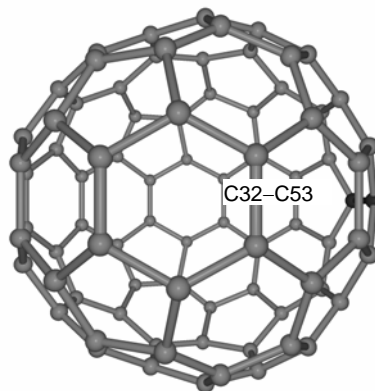
Description of the 126 C–C bonds of the D_{2d} -C₈₄:23 IPR isomer divided into 19 non-equivalent sets

<i>C–C bond</i> ¹	<i>Ring junction</i>	<i>Type</i> ²	<i>Bond lengths</i> (Å)	θ_p (°) ³	<i>MBO</i>
32,53	6:6	pyracylene, A	1.375	10.80	1.375
9,10	6:6	pyracylene, A	1.369	10.68	1.352
5,6	6:6	pyracylene, A	1.377	10.98	1.325
1,2	6:6	B	1.419	9.32	1.314
7,22	6:6	B	1.416	9.68	1.265
12,13	6:6	B	1.413	8.80	1.255
13,31	6:5	corannulene, D	1.424	10.16	1.255
11,12	6:6	B	1.427	9.30	1.249
21,41	6:6	B	1.423	9.67	1.244
7,8	6:5	corannulene, D	1.428	10.67	1.234
2,3	6:6	pyrene, C	1.461	7.67	1.196
1,6	6:5	corannulene, D	1.431	10.97	1.176
21,22	6:6	pyrene, C	1.468	8.73	1.156
2,12	6:6	pyrene, C	1.465	7.78	1.154
1,9	6:5	corannulene, D	1.445	10.83	1.128
5,20	6:5	corannulene, D	1.453	10.81	1.115
23,43	6:5	corannulene, D	1.446	10.71	1.117
8,9	6:5	corannulene, D	1.444	10.70	1.132
13,14	6:5	corannulene, D	1.456	9.71	1.099

Schlegel diagram showing the numbering system for $D_{2d}\text{-C}_{84}$:**23** (a) and structure with the C32–C53 bond marked (b)



(a) Schlegel diagram of $D_{2d}\text{-C}_{84}$:**23**



(b) Structure of $D_{2d}\text{-C}_{84}$:**23**

REFERENCES AND NOTES

¹ Systematic numeric system from reference Taylor, R. *J. Chem. Soc., Perkin Trans. 2* **1993**, 813.

² See A.1 for a schematic representation of the different motifs: pyracylene **A**, **B**, pyrene **C**, corannulene **D**, pentalene **E** and **F** types.

³ Average pyramidalization angle of each carbon atom in the carbon bond.

⁴ Mayer Bond Order (MBO).

⁵ Average values from a D_{2h} symmetry used in the calculation.

index of figures

Figura 1.1	Estructura geomètrica de 4 dels 5 isòmers IPR del C_{78}	12
Figura 1.2	Estructura geomètrica de 6 dels 7 isòmers IPR del C_{80}	14
Figura 1.3	Energia per àtom (EPA) pels isòmers IPR més estables de les estequiometries compreses entre el C_{60} i el C_{84} (cercles plens) i alguns altres isòmers involucrats en aquest treball (quadrats buits)	16
Figure 4.1	Optimized structures for $Sc_3N@C_{78}$: 1 (a), $Sc_3N@C_{80}$: 11 (b) and $Sc_3N@C_{68}$ (c)	72
Figure 4.2	Orbital interaction diagram for $Sc_3N@C_{78}$: 1 and $Sc_3N@C_{80}$: 11	76
Figure 4.3	Electron density deformation map (EDDM) for $Sc_3N@C_{78}$: 1 (a) and $Sc_3N@C_{80}$: 11 (b)	79
Figure 4.4	3D representations, symmetries, energies (in eV) and composition (% Sc_3N / % cage) of the most important molecular orbitals (MOs) involved in the electron charge transfer and in the ionic metal bond for the $Sc_3N@C_{78}$: 1 and $Sc_3N@C_{80}$: 11 optimized complexes	83
Figure 4.5	Carbon chains, symmetries, isomer number and relative energies (RE, in eV) with schematic positions of the scandiums with respect to the pyracylene C–C bond types for the $Sc_3N@C_{78}$ optimized isomers ...	85
Figure 4.6	In-plane bonding interaction between a Sc metal and a 6:6 C–C bond in $Sc_3N@C_{78}$: 1 isomer (a) and non-bonding interaction between a Sc metal and a 6:5 C–C bond in $Sc_3N@C_{78}$: 4 isomer (b)	87
Figure 4.7	Carbon chains, symmetries, isomer number and relative energies (RE, in eV) with schematic position of scandiums in a 2D representation for the $Sc_3N@C_{80}$ optimized isomers	89
Figure 4.8	Vertical ionization potentials (IPs) and vertical electron affinities (EAs) versus HOMO and LUMO energies, respectively, for the free C_{60} , D_3-C_{68} : 6140 , $D_{3h}-C_{78}$: 5 , I_h-C_{80} : 7 and their TNT endohedral metallofullerenes: $Sc_3N@C_{68}$, $Sc_3N@C_{78}$: 1 and $Sc_3N@C_{80}$: 11	93
Figure 4.9	Optimized structures for $M_3N@C_{78}$: 1 (M = Sc (a), Y (b) and La (c)) and $M_3N@C_{80}$: 11 (M = Sc (d), Y (e) and La (f))	96
Figure 4.10	The ionic bond between the trimetallic nitride template (TNT) and the fullerene cages: D_3-C_{68} : 6140 , $D_{3h}-C_{78}$: 5 and I_h-C_{80} : 7	101
Figure 4.11	Why only D_3-C_{68} : 6140 , $D_{3h}-C_{78}$: 5 , I_h-C_{80} : 7 and $D_{5h}-C_{80}$: 6 encapsulate TNT units	103
Figure 4.12	Evolution of the three most reactive exohedral sites (bold lines) for I_h-C_{80} : 7 and $Sc_3N@C_{80}$ isomers according to pyramidalization angle	

	(θ_p) and Mayer bond order (MBO) analysis drawn in the Schlegel diagram of I_h -C ₈₀ :7	114
Figure 4.13	Structure for the most stable Sc ₃ N@C ₈₀ -C ₄ H ₆ isomer (a) and for the X-ray of Sc ₃ N@C ₈₀ -C ₁₀ H ₁₀ O ₂ (b)	119
Figure 4.14	The three most reactive exohedral sites for D_{3h} -C ₇₈ :5 (a) and Sc ₃ N@C ₇₈ :1 (b) drawn in the Schlegel diagram	121
Figure 4.15	The three most reactive exohedral sites for D_3 -C ₆₈ :6140 (a) and Sc ₃ N@C ₆₈ (b)	123
Figure 4.16	Schlegel diagram for the I_h -C ₈₀ :7 fullerene showing numbering	125
Figure 4.17	Optimized structure (a) and Schlegel diagram (b, ● = H) for C ₈₀ H ₄₄	128
Figure 4.18	Hydrogenation binding energy per added H ₂ (HBE/ <i>n</i>) for series C ₈₀ H _{<i>x</i>} (<i>x</i> = 2, 4, 16, 36, 44, 48, 52, 72, 76, 78 and 80), circles, and Sc ₃ N@C ₈₀ H _{<i>x</i>} (<i>x</i> = 44, 48, 52, 72), squares	131
Figures 4.19	Optimized structure (a) and the Schlegel diagram (b, ● = H) for C ₈₀ H ₅₂ :1	135
Figure 4.20	Optimized structures for Sc ₃ N@C ₈₀ H ₅₂ :1 (a) and Sc ₃ N@C ₈₀ H ₅₂ :5 (b)	136
Figure 4.21	Optimized structure (a) and Schlegel diagram (b, ● = H) for C ₈₀ H ₅₂ :5	137
Figure 4.22	The three highest occupied molecular orbitals of Sc ₃ N@C ₈₀ H ₅₂ :5	139
Figure 5.1	Two perspective visions of the C _{2v} -C ₅₈ Pt (a) (substitution at 6:6 C–C bond) and C _s -C ₅₈ Pt (b) (substitution at 6:5 C–C bond) isomers	160
Figure 5.2	Differences between the substitution of a pyracylene 6:6 C–C bond (a) and a corannulene 6:5 C–C bond (b) for a Pt atom in C ₆₀	163
Figure 5.3	Optimized structure for D_{4h} -C ₂₄ H ₁₂ Pt, used as a bonding model for C _{2v} -C ₅₈ Pt	166
Figure 5.4	Molecular orbital (MO) correlation diagram for π interaction system between Pt (left, 4 <i>d</i> electrons in two metal orbitals) and C ₂₄ H ₁₂ (right, 4 <i>p_z</i> electrons + 2 additional electrons in three carbon ligand orbitals) for the D_{4h} -C ₂₆ H ₁₂ Pt compound	167
Figure 5.5	Molecular orbital (MO) correlation diagram for σ interaction system between Pt (left, 6 <i>d</i> electrons in three metal orbitals) and C ₂₄ H ₁₂ (right, 4 <i>sp</i> ² electrons in two carbon ligand orbitals) for D_{4h} -C ₂₆ H ₁₂ Pt	169
Figure 5.6	Evolution of the molecular orbitals (MOs) of the interaction between a tetracoordinated Pt atom and four carbons with 4 <i>p_z</i> electrons and 4 <i>sp</i> ² electrons from D_{4h} -C ₂₄ H ₁₂ Pt to C _{4v} -C ₂₄ H ₁₂ Pt and C _{2v} -C ₂₄ H ₁₂ Pt	171

Figure 5.7	The most important molecular orbitals (MOs) of C_{2v} - $C_{58}Pt$:66	172
Figure 5.8	Correlation between cage radius and HOMA versus the substitution energy (SE) for C_{2v} - $C_{58}M$ and C_s - $C_{58}M$ ($M = Pt, Ir, Os, Ti$)	176
Figure 5.9	Optimized structure for $[C_{58}Ir(C_2H_4)]^-$	184
Figure 5.10	Molecular orbital (MO) correlation diagram for the interaction between C_2H_4 ligand (right) and $C_{58}Ir^-$ (left) in order to construct the $[C_{58}Ir(C_2H_4)]^-$ complex	186
Figure 5.11	3D representation of the HOMO of $[C_{58}Ir(C_2H_4)]^-$	188
Figure 5.12	Schlegel diagram showing the numbering system for C_{60} (a) and regioisomers of $C_{57}Pt_2$ (b)	193
Figure 5.13	Relationship between Pt–Pt separation and stability of the different regioisomers of $C_{57}Pt_2$	195
Figure 5.14	Different views of the optimized structure of the most stable $C_{57}Pt_2$:11 regioisomer	196
Figure 5.15	Schlegel diagram showing the numbering system for regioisomers of $C_{56}Pt_2$	198
Figure 5.16	Different views of the optimized structure of the most stable $C_{56}Pt_2$:10 regioisomer	199
Figure 5.17	Schematic representation of the platinum atoms coordination in regioisomers of $C_{57}Pt_2$ and $C_{56}Pt_2$ that the platinum-platinum distance is lower than 3 Å	204
Figure 5.18	<i>Biplot</i> for regioisomers of $C_{57}Pt_2$ obtained after PLS regression on the nine factors of Table 5.17	212
Figure 5.19	DFT calculated versus PLS predicted relative energy (RE) obtained from the PLS regression model on the nine studied factors of $C_{57}Pt_2$	215
Figure 5.20	<i>Biplot</i> for regioisomers of $C_{56}Pt_2$ obtained after PLS regression on the nine factors of Table 5.18	216
Figure 5.21	Schlegel Diagram showing the numbering system for D_{2d} - C_{84} :23 fullerene and regioisomers of $C_{81}Pt_2$	218
Figure 5.22	DFT calculated versus PLS predicted relative energy (RE) obtained from the PLS regression model on the four topological factors of $C_{57}Pt_2$	221
Figure 5.23	Ionization potentials (IPs) and electron affinities (EAs) versus HOMO and LUMO energies, respectively, for the free C_{60} and $C_{58}Pt$, $C_{59}Pt$, $C_{56}Pt_2$ and $C_{57}Pt_2$ heterofullerenes	224
Figure 6.1	Schlegel diagram (a) and molecular structure (b) of the D_{5h} - C_{70} :1 that incorporate the different set of C–C bonds studied	238

Figure 6.2	Schlegel diagram (a) and molecular structure (b) of the D_{2d} - C_{84} :23 isomer that incorporate the different set of C–C bonds studied	239
Figure 6.3	Schlegel diagram (a) and molecular structure (b) of the D_2 - C_{84} :22 isomer that incorporate the different set of C–C bonds studied	240
Figure 6.4	The structure of the most stable isomers of $(\eta^2-C_{60})Pt(PH_3)_2$, metal unit linked to the 6:6 C–C bond type (a); $(\eta^2-C_{70})Pt(PH_3)_2$, metal unit linked to the Ca–Cb bond (b), and $(\eta^2-C_{84})Pt(PH_3)_2$, metal unit linked to the C42–C43 bond (c)	249
Figure 6.5	Correlation between the binding energy (BE) and the pyramidalization angle (θ_p) for $(\eta^2-C_n)\{M(PH_3)_2\}_n$ ($M = Pt, Pd, Ni; n = 2, 4, 6$)	255
Figure 6.6	Mayer bond order (MBO) versus fullerene-metal binding energies (BE) for the C_{60} , C_{70} and C_{84} complexes	264
Figure 6.7	Pyramidalization angle (θ_p) versus fullerene-metal binding energies (BE) for the C_{60} , C_{70} and C_{84} complexes	265
Figure 6.8	Free C–C bond distance versus fullerene-metal binding energies (BE) for the C_{60} , C_{70} and C_{84} complexes	266

index of tables

Taula 1.1	Caracterització electrònica i geomètrica dels isòmers IPR més estables entre el C_{60} i el C_{84} i alguns altres fullerenes d'interès pel treball d'investigació	15
Taula 2.1	Versió de l'ADF emprada i formalisme aplicat en les correccions relativistes en cadascun dels capítols	44
Taula 2.2	Llista completa dels elements que apareixen en els càlculs dels capítols 4-6 amb els seus respectius electrons de <i>core</i> . Tots els electrons de valència són descrits per conjunts de base STO de qualitat triple- ζ + polarització (TZP)	45
Table 4.1	Comparison of some computed and experimental bond lengths for the most stable isomers of $Sc_3N@C_{68}$, $Sc_3N@C_{78}$ and $Sc_3N@C_{80}$ endohedral metallofullerenes	74
Table 4.2	Mulliken populations for the Sc_3N unit in several TNT endohedral metallofullerenes	78
Table 4.3	Decomposition of the encapsulation binding energy (EBE) for the most stable $Sc_3N@C_k$ ($k = 68, 78, 80$) isomers	80
Table 4.4	Decomposition of the encapsulation binding energy (EBE) for the $Sc_3N@C_{78}$ optimized isomers	86
Table 4.5	Decomposition of the interaction energy (ΔE_{INT}) for the $Sc_3N@C_{78}$ model complexes	88
Table 4.6	Comparison of some computed and experimental bond lengths for several $Sc_3N@C_{80}$ isomers	91
Table 4.7	Vertical ionization potentials (IPs) and electron affinities (EAs) for several optimized molecules	92
Table 4.8	Geometric properties for $M_3N@C_k$ ($M = Sc, Y, La; k = 68, 78, 80$) endohedral complexes	94
Table 4.9	Decomposition of the encapsulation binding energy (EBE) for the $M_3N@C_k$ ($M = Sc, Y, La; k = 68, 78, 80$)	98
Table 4.10	Description of the thirty-four distinct set of C–C bonds of the C_{2v} - $Sc_3N@C_{80}:\mathbf{6}$ isomer	109
Table 4.11	Description of the sixty-four distinct set of C–C bonds of the C_s - $Sc_3N@C_{80}:\mathbf{11}$ isomer	110
Table 4.12	Description of the sixty-four distinct set of C–C bonds of the C_s - $Sc_3N@C_{80}:\mathbf{12}$ isomer	112

Table 4.13	Geometric properties and relative energies (REs) for $\text{Sc}_3\text{N}@C_{80}\text{-C}_4\text{H}_6$ and $\text{C}_{80}\text{-C}_4\text{H}_6$ isomers	116
Table 4.14	Crucial geometric parameters which change during the derivatization via a [4 + 2] cycloaddition reaction on $\text{Sc}_3\text{N}@C_{80}$: 12 isomer	117
Table 4.15	Change of the characteristics of the thirteen different set of C–C bonds from the free D_{3h} - C_{78} : 5 (initial) to the $\text{Sc}_3\text{N}@C_{78}$: 1 (final)	120
Table 4.16	Change of the characteristics of the thirteen different set of C–C bonds from the free D_3 - C_{68} : 6140 (initial) to the $\text{Sc}_3\text{N}@C_{68}$ (final)	122
Table 4.17	Hydrogenation binding energies (HBE/ <i>n</i> , eV) per added H_2 of the most stable C_{80}H_x and $\text{Sc}_3\text{N}@C_{80}\text{H}_x$ isomers	126
Table 4.18	Deformation (ΔE_{DE}) and interaction energy (ΔE_{INT}) components of the hydrogenation binding energies per added H_2 (HBE/ <i>n</i>) for the most stable isomers of C_{80}H_x	129
Table 4.19	Decomposition of the hydrogenation (HBE) and encapsulation (EBE) binding energies for $\text{Sc}_3\text{N}@C_k$ (<i>k</i> = 78, 80) and $\text{Sc}_3\text{N}@C_{80}\text{H}_x$ (<i>x</i> = 44, 48, 52, 72)	130
Table 4.20	Description and relative energies (RE) of $\text{C}_{80}\text{H}_{52}$, $\text{C}_{80}\text{F}_{52}$ and $\text{Sc}_3\text{N}@C_{80}\text{H}_{52}$ isomers	133
Table 4.21	Optimized distances for $\text{Sc}_3\text{N}@C_{80}\text{H}_{52}$ isomers	138
Table 4.22	Relative binding energies (RE[HBE] and RE[EBE]) for the most stable $\text{Sc}_3\text{N}@C_{80}\text{H}_{52}$ isomers	140
Table 5.1	Geometric and electronic properties for C_{59}Pt , $\text{C}_{2v}\text{-C}_{58}\text{Pt}$, $\text{C}_s\text{-C}_{58}\text{Pt}$ and $\text{C}_{24}\text{H}_{12}\text{Pt}$	161
Table 5.2	Decomposition of the substitution energy (SE) for $\text{C}_{2v}\text{-C}_{58}\text{Pt}$ and $\text{C}_s\text{-C}_{58}\text{Pt}$ and $D_{4h}\text{-C}_{24}\text{H}_{12}\text{Pt}$	162
Table 5.3	Decomposition of the orbital interaction term (ΔE_{ORB}) for $D_{4h}\text{-C}_{24}\text{H}_{12}\text{Pt}$, $\text{C}_{2v}\text{-C}_{58}\text{Pt}$ and $\text{C}_s\text{-C}_{58}\text{Pt}$ in the irreducible representation of each symmetry	174
Table 5.4	Geometric properties for $\text{C}_{2v}\text{-C}_{58}\text{M}$ and $\text{C}_s\text{-C}_{58}\text{M}$ (<i>M</i> = Pt, Ir, Os) ...	175
Table 5.5	Decomposition of the substitution energy (SE) for $\text{C}_{2v}\text{-C}_{58}\text{M}$ and $\text{C}_s\text{-C}_{58}\text{M}$ (<i>M</i> = Pt, Ir, Os)	178
Table 5.6	Characterization of the eight distinct regioisomers of C_{68}Pt , a doped fullerene from the free $D_{5h}\text{-C}_{70}$: 1	179
Table 5.7	Geometric properties for C_{59}M (<i>M</i> = Pt, Ir, Os, Ti)	181
Table 5.8	Decomposition of the substitution energy (SE) for C_{59}M (<i>M</i> = Pt, Ir, Os)	182
Table 5.9	Substitution energy (SE) for cation, neutral and anion C_xM (<i>x</i> = 58, 59; <i>M</i> = Pt, Ir, Os) clusters	183

Table 5.10	Geometric and electronic properties for cation, neutral and anion $C_{58}Ir(C_2H_4)$ and $C_{58}Pt(C_2H_4)$ complexes	185
Table 5.11	Decomposition of the binding energy (BE) for $C_{58}Ir(C_2H_4)$	189
Table 5.12	Decomposition of the binding energy (BE) for $C_{58}Pt(C_2H_4)$	191
Table 5.13	Description and numbering scheme for regioisomers of $C_{57}Pt_2$	194
Table 5.14	Description and numbering scheme for regioisomers of $C_{56}Pt_2$	199
Table 5.15	Substitution energy (SE) and bonding energy (BE) per atom for mono- and diheterofullerenes	201
Table 5.16	Several parameters for determining the bonding character of the platinum-platinum bond	203
Table 5.17	Geometric factors and relative energies (REs) for regioisomers of $C_{57}Pt_2$	210
Table 5.18	Geometric factors and relative energies (REs) for regioisomers of $C_{56}Pt_2$	211
Table 5.19	Regression coefficients of PLS model considering two latent variables	214
Table 5.20	Relative energies (REs) for different clusters: $C_{56}Pt_2$, $C_{56}Pt_2^+$, $C_{56}Pt_2^-$, $C_{56}Ti_2$ and C_{56}	217
Table 5.21	PLS prediction of isomer stability of $C_{81}Pt_2$, a doped heterofullerene from the $D_{2d}-C_{84}$: 23 isomer	220
Table 5.22	Ionization potentials (IPs) and electron affinities (EAs) for several mono- and diheterofullerenes	223
Table 6.1	Description of A-B interactions, A is a ligand and B is a molecule containing a metal atom	243
Table 6.2	Decomposition of the binding energy (BE) for series that represents A-B interactions	246
Table 6.3	DFT geometries and binding energies (BE) for the $(\eta^2-C_{60})Pt(PH_3)_2$ complex and for the $(\eta^2-C_{14}H_8)Pt(PH_3)_2$ and $(\eta^2-C_2H_4)Pt(PH_3)_2$ model complexes	250
Table 6.4	DFT geometries and binding energies (BE) for $(\eta^2-C_{60})M(PH_3)_2$ and $(\eta^2-C_2H_4)M(PH_3)_2$ (M = Pd, Ni)	251
Table 6.5	Comparison of the various calculated and experimental BE of $(\eta^2-C_2H_4)M(PH_3)_2$ (M = Pt, Pd, Ni) ethylene complexes	252
Table 6.6	Geometric properties and fullerene-metal binding energies (BE) for $(\eta^2-C_{60})\{Pt(PH_3)_2\}_n$ (n = 1, 2, 4, 6)	254
Table 6.7	Geometric properties and fullerene-metal binding energies (BE) for $(\eta^2-C_{60})\{Pd(PH_3)_2\}_n$ (n = 1, 2, 4, 6)	256

Table 6.8 Geometric properties and fullerene-metal binding energies (BE) for (η^2 - C_{60}) $\{Ni(PH_3)_2\}_n$ (n = 1, 2, 4, 6)	257
Table 6.9 Geometric properties and binding energies (BE) for (η^2 - C_{70})Pt(PH ₃) ₂ and (η^2 - C_{84})Pt(PH ₃) ₂	259
Table 6.10 Mulliken net charges for several Pt(PH ₃) ₂ exohedral metallofullerenes	262

general index

Prefaci [CAT]	ix
Contents [ENG]	xv
List of publications [ENG]	xix
List of abbreviations and symbols [ENG]	xxi

PART I. INTRODUCCIÓ [CAT] 1

1 QUÍMICA DE FUL·LERENS	3
1.1 Introducció	6
1.2 Ful·lerens lliures	7
1.2.1 <i>Ful·lerens com a poliedres</i>	7
1.2.2 <i>Compromís entre la corbatura i l'estructura electrònica</i>	8
1.2.3 <i>Regla dels pentàgons aïllats (IPR)</i>	9
1.2.4 <i>Isòmers dels ful·lerens IPR</i>	10
1.2.5 <i>Obtenció experimental</i>	13
1.3 Caracterització	15
1.3.1 <i>Estabilitat en l'increment de carbonis</i>	15
1.3.2 <i>Propietats geomètriques</i>	17
1.3.3 <i>Estructura electrònica</i>	18
1.3.4 <i>Aromaticitat</i>	19
1.3.5 <i>Propietats físiques</i>	20
1.3.6 <i>Reactivitat química</i>	21
1.4 Metal·loful·lerens	22
1.4.1 <i>Endoèdrics</i>	23
1.4.2 <i>Heteroèdrics</i>	24
1.4.3 <i>Exoèdrics</i>	25
Referències i notes	26
2 QUÍMICA COMPUTACIONAL PER FUL·LERENS	31
2.1 Introducció	33
2.2 Mètodes semiempírics	35
2.3 Aproximació Hartree-Fock (HF)	36

2.4	Teoria del funcional de la densitat (DFT)	39
2.5	Detalls computacionals	43
2.5.1	<i>Funcionals de la densitat</i>	43
2.5.2	<i>Funcions de base</i>	44
2.6	Eines per l'anàlisi	45
2.6.1	<i>Descomposició de l'energia d'enllaç (BE)</i>	46
2.6.2	<i>Càrregues atòmiques</i>	47
2.6.3	<i>Mapes de deformació de la densitat electrònica (EDDM)</i>	47
2.6.4	<i>Àtoms a les molècules (AIM)</i>	48
2.6.5	<i>Anàlisi multivariant de dades</i>	48
	Referències i notes	50

3 ABAST I OBJECTIUS DE LA TESI 55

3.1	Metal·loful·lerens endoèdrics	56
3.2	Metal·loful·lerens heteroèdrics	57
3.3	Metal·loful·lerens exoèdrics	59

PART II. RESULTS [ENG] 61

4 TNT ENDOHEDRAL METALLOFULLERENES 63

4.1	Introduction	67
4.1.1	<i>Experimental part</i>	67
4.1.2	<i>Theoretical part</i>	69
4.2	Ionic bond between the fullerene cage and the trimetallic nitride template (TNT)	70
4.2.1	<i>Structures of $Sc_3N@C_k$ ($k = 68, 78, 80$)</i>	70
4.2.2	<i>Ionic model</i>	76
4.2.3	<i>Electron charge transfer</i>	78
4.2.4	<i>Decomposition of the encapsulation binding energy (EBE)</i>	80
4.3	Isomerism	84
4.3.1	<i>$Sc_3N@C_{78}$</i>	84
4.3.2	<i>$Sc_3N@C_{80}$</i>	90
4.4	Physical properties	91

4.5	Extended family: $M_3N@C_k$ ($M = La, Y; k = 78, 80$)	93
4.5.1	<i>Experimental considerations</i>	93
4.5.2	<i>Geometry considerations</i>	95
4.5.3	<i>Electronic structure</i>	95
4.5.4	<i>Decomposition of the EBE</i>	97
4.6	General rule for the stabilization of cages encapsulating TNT units	99
4.6.1	<i>The stability can be predicted</i>	99
4.6.2	<i>Bond resonance energy method</i>	100
4.6.3	<i>LUMO+3–LUMO+4 gap method</i>	101
4.7	Exohedral reactivity (I): [4 + 2] cycloaddition	103
4.7.1	<i>Experimental and theoretical considerations</i>	104
4.7.2	<i>Effects of TNT encapsulation on exohedral reactivity</i>	105
4.7.3	<i>[4 + 2] cycloaddition on $Sc_3N@C_{80}$</i>	115
4.7.4	<i>Clues about [4 + 2] cycloaddition on $Sc_3N@C_k$ ($k = 68, 78$)</i>	119
4.8	Exohedral reactivity (II): fluorination of $Sc_3N@C_{80}$	124
4.8.1	<i>Experimental part</i>	124
4.8.2	<i>Hydrogenation binding energies (HBE) for I_h-C_{80}</i> ..	124
4.8.3	<i>HBE for $Sc_3N@C_{80}$</i>	129
4.8.4	<i>Sc_3N encapsulation in free cages vs. hydrogenated fullerenes</i>	130
4.8.5	<i>Stabilities of $C_{80}H_{52}$ and $C_{80}F_{52}$ isomers</i>	132
4.8.6	<i>Stabilities of $Sc_3N@C_{80}H_{52}$ isomers</i>	134
4.8.7	<i>Geometric and electronic structure of $Sc_3N@C_{80}H_{52}:5$</i>	135
4.8.8	<i>Factors affecting the stabilization energies</i>	138
4.9	Concluding remarks	141
	References and notes	146
5	HETEROHEDRAL METALLOFULLERENES	153
5.1	Introduction	157
5.1.1	<i>Experimental part</i>	157
5.1.2	<i>Theoretical part</i>	158
5.2	Covalent metal bond in the fullerene carbon framework	159

5.2.1	<i>Geometric and electronic structure of C₅₈Pt</i>	159
5.2.2	<i>Substitution energy (SE) and its decomposition</i>	161
5.2.3	<i>Hole energy, ΔE_{HOLE}</i>	164
5.2.4	<i>Insertion binding energy (IBE)</i>	164
5.2.5	<i>Fragment molecular orbital method</i>	165
5.3	Monoheterofullerenes: C ₅₈ M, C ₅₉ M (M = Pt, Ir, Os, Ti) and C ₆₈ Pt	174
5.3.1	<i>C₅₈M (M = Pt, Ir, Os, Ti)</i>	174
5.3.2	<i>C₆₈Pt, a doped fullerene from D_{5h}-C₇₀</i>	178
5.3.3	<i>C₅₉M (M = Pt, Ir, Os, Ti)</i>	180
5.3.4	<i>Stability of neutral monoheterofullerenes versus cation and anion analogues</i>	183
5.4	Addition of ethylene to monoheterofullerenes	184
5.4.1	<i>Experimental evidence</i>	184
5.4.2	<i>Interaction between ethylene and monoheterofullerenes</i>	185
5.5	Diheterofullerenes: C ₅₇ Pt ₂ , C ₅₆ Pt ₂ and C ₈₁ Pt ₂	192
5.5.1	<i>Regioisomers of C₅₇Pt₂</i>	193
5.5.2	<i>Regioisomers of C₅₆Pt₂</i>	197
5.5.3	<i>Electronic structure</i>	200
5.5.4	<i>Metal-metal coupling</i>	202
5.5.5	<i>Topological and structural factors that govern isomer stability</i>	205
5.5.6	<i>Chemometric study of the structure-energy relationship</i>	211
5.5.7	<i>Stability of the carbon skeleton is the principal factor that determines the isomer stability</i>	215
5.5.8	<i>Prediction of isomer stability of C₈₁Pt₂, a doped fullerene from D_{2d}-(C₈₄:23)</i>	218
5.6	Physical properties	222
5.7	Concluding remarks	223
	References and notes	228
6	M(PH₃)₂ EXOHEDRAL METALLOFULLERENES	233
6.1	Introduction	236
6.1.1	<i>Experimental part</i>	236

6.1.2 Theoretical part	238
6.2 Coordination bond between the fullerene cage and the metal unit	241
6.2.1 Structure of (η^2 -C ₆₀)Pt(PH ₃) ₂	241
6.2.2 The Dewar-Chatt-Duncanson model	244
6.3 Monoaddition complexes of C ₆₀ and ethylene	247
6.3.1 Pt complexes	247
6.3.2 Pd and Ni complexes	251
6.4 Polyaddition complexes of C ₆₀	253
6.4.1 Energy and geometry considerations of Pt complexes	253
6.4.2 Pd and Ni complexes	256
6.4.3 Pyramidalization angle of carbons attached to the metal unit	257
6.5 Monoaddition complexes of C ₇₀ and C ₈₄	258
6.5.1 C ₇₀	258
6.5.2 C ₈₄	260
6.5.3 Electron charge transfer	263
6.6 Prediction of the most reactive sites	263
6.7 Concluding remarks	266
References and notes	269
7 FINAL CONCLUSIONS	273
7.1 Conclusions	273
7.2 Perspectives	278
Appendix [ENG]	281
A.1 General description	282
A.2 I _h -C ₆₀ : 1	283
A.3 D ₃ -C ₆₈ : 6140	284
A.4 D _{5h} -C ₇₀ : 1	286
A.5 D _{3h} -C ₇₈ : 5	287
A.6 I _h -C ₈₀ : 7	289
A.7 D ₂ -C ₈₄ : 22	290
A.8 D _{2d} -C ₈₄ : 23	292
References and notes	293

Index of figures [ENG]	295
Index of tables [ENG]	299
General index [ENG]	303
Agraïments [CAT]	309
Viatges [CAT]	313

agraïments

Tot gran viatge té una tripulació que surt a navegar faci mala mar o resplendeixi el sol més paradisiac. He d'agrair els que em van guiar inicialment en aquest viatge, quan jo ja era mariner sense vaixell esperant al port: la Rosa, el Ricart, el Joan, la Mar, l'Anna i especialment els capitans que m'embarcaren a la seva flota: en Josep Maria Poblet i en Carles Bo. Sempre recordaré amb nostàlgia la constància del primer i les mirades a l'horitzó del segon. A cada mariner se li assignava un vaixell i després d'un temps inspeccionant l'estribord i el babord tots acabàvem a la sala de màquines. La meva flota estava plena de vaixells, alguns ja portaven anys navegant i d'altres començaven, com jo. Tots els vaixells havíem salpat amb les veles esteses dins una mar immensa de color blau. Mentre navegàvem no ens veiem gaire però sempre recordarem les nits sota la embriagadora lluna a coberta o al camarot, al port, o alguna illa dita Sevilla i/o Barcelona o a la ciutat. Bons mariners sense dubte: el Xavi, el Jose, el Joan Miquel, el Jorge, l'Anaval, el Paco, l'Alfred, el Gerard, el Jesuset, l'Isa, l'Esther, l'Helena, la Susanna, el David, l'Elias i la Núria. Tots érem peculiars: alguns els hi agradava més muntar veles que navegar i d'altres tenien molta experiència en la navegació. Alguns passaven més temps a terra que a mar i d'altres sempre d'illa en illa. De tots ells en tinc un granet. Els mariners Elias i Núria eren del mateix escamot que el meu, de fet, vàrem salpar plegats. Quantes tempestes i alegries junts! Sempre teníem temps per anar a esvalotar el galliner del port! Ara crec que toca el de la ciutat, oi? Què faria un vaixell sense uns bons oficials de manteniment? Pregunteu-li al capità James S. Hook! Doncs, res. Quantes vegades ens han salvat d'un naufragi segur! El Jose, el Joan i l'Elisenda! Gràcies per mantenir els vaixells en bones condicions. D'altres portaven el paperam amb la cort (Yolanda) o bé revisaven el complex estilisme marcat per l'època (John). Quan portaves moltes dies de navegació sense tornar a port podies perdre't. A vegades era bo perdre't per la mar i deixar-te endur per alguna tempesta que de ben segur a algun lloc nou et portava. En aquestes escapades vaig acabar a tres illes força interessants: *Bath*, *Exeter* i *Sussex*. En cada illa vaig aprendre coses diferents. Ara penso que tothom hauria de tenir l'oportunitat de visitar-ne alguna, d'illa. No cal ser en *Robinson Crusoe* per fer-ho! La primera illa la vaig trepitjar molt cautelosament sense saber què i qui em

trobaria. Quin mariner seria jo sense les tècniques de navegació turques de *Bath*? Ebru, Yudum i Mete, molta sort *and see you later!* A l'illa de *Bath* vaig també forjar l'amistat amb un mariner de terra endins: el Pedret. *Una Pizza, please! We need a change!* A *Exeter* vaig fer una parada curta però profitosa, necessitava una mica de coco de platja: la Rosa, l'Helena i la Rakel em van acompanyar. Quines andorranes! Finalment en l'última illa vaig conèixer els nadius. Fins i tot em van allotjar. Una forta abraçada per la càlida acollida de la família de la Doreen: Hugh, Suzanne, Ethan, Owain i Lydia. *I was like a brother! Thank you!* Tot i les aventures dignes d'un *Indiana Jones*: Arribada d'un *keimpa* a Sussex, a la recerca de les bases perdudes de Newcastle, el congrès fantasma d'Exeter, el projecte *Hirsch-Erlangen*: si tu no vols jo vinc, ful·lerens a *Methyl Tydfil* i la *Hadrian's Wall?*, el pis cinquè, *London* la no-capital, els trens sense rumb per la hispània ulterior, per què tres catalans no es troben a la mateixa hora i el mateix lloc?, el *Sherlock Holmes* de Lewes, de *James Bond* a l'Opera de *Glyndebourne*, creuer pel mississipí baètic ... i un llarg etcètera al final sempre vaig tornar a casa. Així doncs, tot mariner té uns dies a alta mar i altes a terra ferma. A terra ferma aprofitava per copsar l'opinió que sovint la llunyania de la mar no em deixava veure. Quant he après de la Montse, la Neus de Tarragona, el Carles i la Cruset de Reus, el Pedret de Montbrí, el Benito de Valls, el Pepe de Cambrils, el Xiquelo de la Ràpita, el Saki de l'Hospi, el Toni d'Orta, la Brezo de Tarragona, la Salla dels Omells de na Gaia, el Saura de Llorenç, el Nino de Bellvei, el Norber de l'Arboç i el Jaume de Santes Creus. Alguns eren amb mi al port a l'inici del viatge. Moltes gràcies a tots! Un que sempre trobava quan tornava era el Gerard. Gràcies per sempre ser-hi! Jo era d'aquells que quan sortia del port i anava a la ciutat, sempre tenia temps per anar a esvalotar-la. Quines estones més maques amb la gent de EL MARGE i el SEP: el Mariano, la Rosa, la Sílvia, el Joan, el Jaume de la Bisbal, l'Andreu i el Joan del Vendrell, la Laura de Masarbonés i el Marc de Llorenç. Els vostres granets mouen muntanyes. A casa del mariner però es coïa tot! A casa era on sempre tenia el refugi i tothom a qualsevol hora m'esperava o em feina la cassola. Quins pares! Sempre al peu del canó, més de terra que no pas de mar! Però il·lusionats que el fill anés a mar! I el meu germà sempre tant treballador fent niuet! Els meus cosins sempre m'esperaven quan tornava a casa amb el sarró: l'Albert i la Montse. Una abraçada a la meva àvia, la padrina, que em va veure

iniciar en aquest món i la meva tieta! I sobretot una mirada de futur als cosinets més xics: el Robert, la Marta, els dos Arnau, l'Aida, la Núria, la Laia i al Roger. Endavant! Entre tant de tràfec, l'Elena m'ha revifat l'ésser humà tant el de muntanya com el de mar, una abraçada i a volar! Però, és clar, fins i tot la mar es pot fer petita si observes atentament allò que vols! A poc a poc vas agafant el rumb i substitueixes els cops de timó per unes bones veles. Jo vaig veure un dia un far molt i molt llunyà i allí em vaig dirigir. Vaig pujar-lo i aquí sóc: ben il·luminat amb unes bones vistes cap a un munt de fars i mars més! On és el proper viatge? i la resta de mariners? Mires enrere i veus el trajecte, ha valgut la pena el camí, oi! Moltes gràcies!

Octubre de 2004
La Bisbal del Penedès / La Masó
Campa xic / *Little Campa*

viatges

Estada al Departament de Química de la Universitat de Bath (Gran Bretanya). Juliol i agost del 2000. Tutor: Dr. Andrew Burrows. Síntesi de fosfines.

Participació en la XVIIena REUNIÓ DE LA XARXA DE QUÍMICA TEÒRICA DE CATALUNYA celebrada a Tarragona el 4 i 5 de juliol del 2001.

Participació i presentació del pòster: "A DFT study of Organometallic Derivatives of Fullerenes, Jordi Muñoz, Josep M. Campanera, Jordi Vázquez, Carles Bo and Josep M. Poblet" en el FIGIPS: MEETING IN INORGANIC CHEMISTRY celebrat entre el 15 i el 20 de juliol de 2001 a Barcelona.

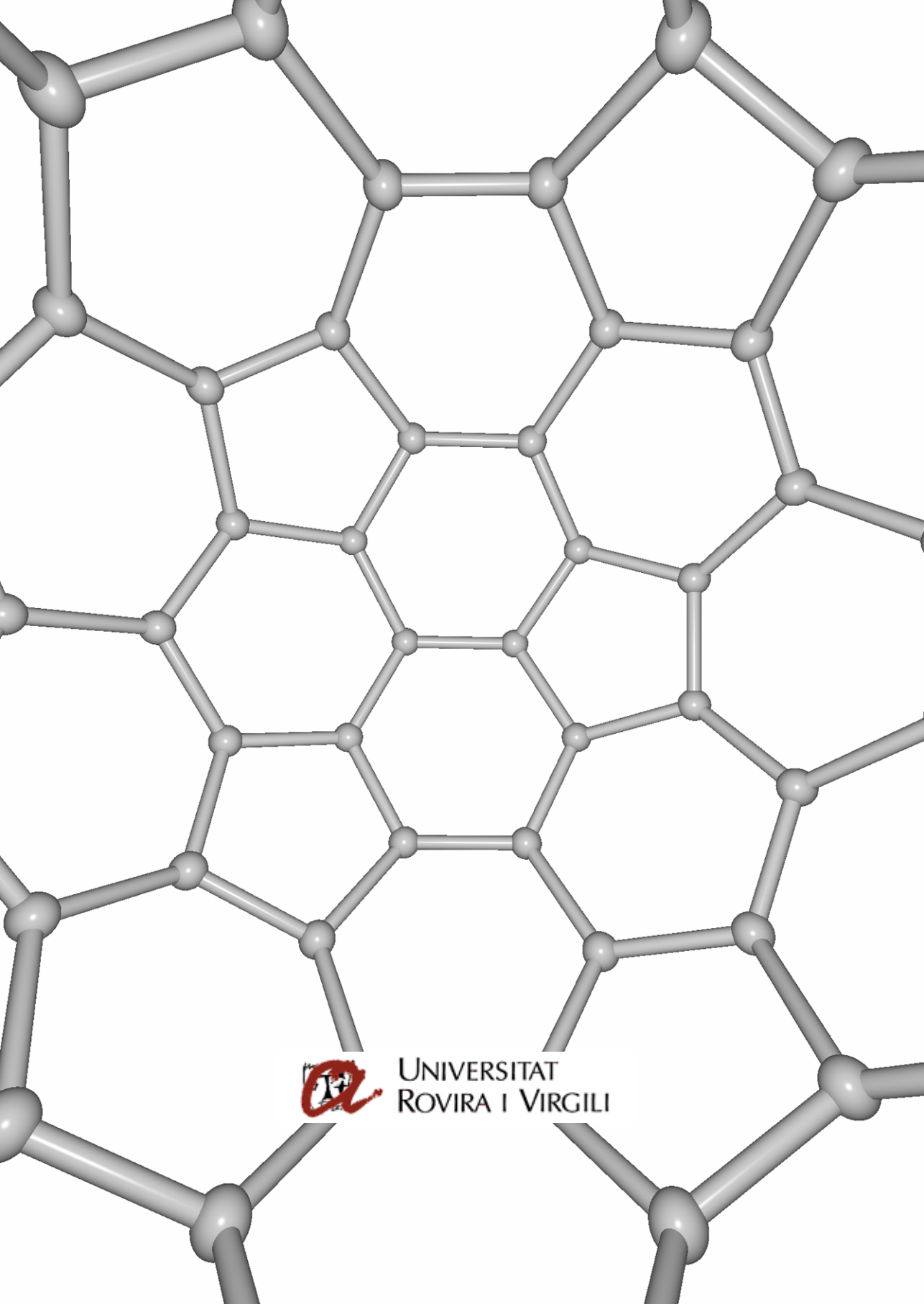
Estada al Departament de Química de la Universitat d'Exeter (Gran Bretanya). Agost del 2001. Tutor: Dr. Craig Butts. Reaccions fotoquímiques de fullerenes.

Participació i presentació de la comunicació. "Enllaç en els endohedres $Sc_3N@C_x$ $x = 68, 78$ i 80 , Josep M. Campanera, Carles Bo, Marilyn M. Olmstead, Alan L. Balch i Josep M. Poblet" en la XVIIIena REUNIÓ DE LA XARXA DE QUÍMICA TEÒRICA DE CATALUNYA que tingué lloc a Barcelona els dies 8 i 9 de juliol de 2002.

Participació i presentació del pòster: "Bonding within the endohedral fullerenes $Sc_3N@C_x$ $x = 68, 78$ and 80 , Josep M. Campanera, Carles Bo, Marilyn M. Olmstead, Alan L. Balch and Josep M. Poblet" a l'ESPA2002: ELECTRONIC STRUCTURE: PRINCIPLES AND APPLICATIONS, celebrat a Sevilla de l'11 al 13 de Setembre de 2002.

Estada al Departament de Química de la Universitat de Sussex (Brighton, Gran Bretanya). Maig-Setembre de 2003. Tutors: Roger Taylor i Malcom Heggie. Analysis of polyaddition levels in *i*- Sc_3NC_{80} .

Participació en la Nanotec'03: NANOTECHNOLOGY IN CARBON RELATED MATERIALS celebrat a la Universitat de Sussex a Brighton (Gran Bretanya) entre el 27 i el 30 d'agost de 2003.



UNIVERSITAT
ROVIRA I VIRGILI